

# The Radiative Forcing Pattern Effect on Climate Sensitivity

Bosong Zhang<sup>1</sup>, Ming Zhao<sup>2</sup>, Haozhe He<sup>3</sup>, Brian Soden<sup>4</sup>, Zhihong Tan<sup>1</sup>, Baoqiang Xiang<sup>5</sup>,  
and Chenggong Wang<sup>1</sup>

<sup>1</sup>Princeton University

<sup>2</sup>GFDL/NOAA

<sup>3</sup>University of Miami

<sup>4</sup>Univ. Miami, Miami

<sup>5</sup>NOAA/Geophysical Fluid Dynamics Laboratory, UCAR

July 20, 2023

## Abstract

This study investigates how climate sensitivity depends upon the spatial pattern of radiative forcing. Sensitivity experiments using a coupled ocean-atmosphere model were conducted by adding anomalous incoming solar radiation over the entire globe, Northern Hemisphere mid-latitudes, Southern Ocean, and tropics, respectively, with both positive and negative perturbation considered. The varied forcing patterns led to highly divergent climate sensitivities, with extratropical forcing inducing significantly more global-mean temperature change compared to tropical forcing. This dependence is particularly strong over the Southern Hemisphere, where the climate is nearly twice as sensitive to Southern Ocean forcing as tropical forcing. This dependence of climate sensitivity on the location of radiative forcing stems from covariations between lapse rate feedback, cloud feedback and tropospheric stability. These results contrast with the conventional SST-pattern effect in which tropical surface temperature changes regulate the climate sensitivity, and has important implications for geoengineering and understanding the mechanisms of paleoclimate change.

## Hosted file

968815\_0\_art\_file\_11187998\_rxydgk.docx available at <https://authorea.com/users/535851/articles/655683-the-radiative-forcing-pattern-effect-on-climate-sensitivity>

## Hosted file

968815\_0\_supp\_11188006\_rxr2zm.docx available at <https://authorea.com/users/535851/articles/655683-the-radiative-forcing-pattern-effect-on-climate-sensitivity>

1                   **The Radiative Forcing Pattern Effect on Climate Sensitivity**  
2

3                   **Bosong Zhang<sup>1</sup>, Ming Zhao<sup>2</sup>, Haozhe He<sup>3</sup>, Brian J. Soden<sup>3</sup>, Zhihong Tan<sup>1</sup>, Baoqiang**  
4                   **Xiang<sup>2</sup>, Chenggong Wang<sup>1</sup>**

5                   <sup>1</sup>Program in Atmospheric and Oceanic Sciences, Princeton University, Princeton, NJ

6                   <sup>2</sup>NOAA/Geophysical Fluid Dynamics Laboratory, Princeton, NJ

7                   <sup>3</sup>Rosenstiel School of Marine, Atmospheric and Earth Science, University of Miami, Miami, FL

8                   Corresponding author: Bosong Zhang (bosongzhang@gmail.com)

9  
10                   **Key points:**

- 11                   • The solar forcing pattern effect is investigated in a coupled ocean-atmosphere model.  
12                   • Climate sensitivity is doubled from tropical forcing to Southern Ocean forcing.  
13                   • The radiative forcing pattern effect involves changes in lapse rate feedback, cloud  
14                   feedback, and tropospheric stability.

15                   **Plain language summary**

16                   The way surface temperature responds to radiative forcing depends on where such  
17                   forcing is applied. The global mean surface temperature change is doubled when the forcing is  
18                   imposed in the tropics compared to when it happens in the mid-latitudes such as the Southern  
19                   Ocean. Changes in the vertical temperature profiles and clouds contribute to the dependence of  
20                   surface temperature change on the forcing geographic locations.

21                   **keywords**

22                   Climate sensitivity; Climate feedback; Radiative forcing pattern effect;

23 **Abstract**

24         This study investigates how climate sensitivity depends upon the spatial pattern of  
25 radiative forcing. Sensitivity experiments using a coupled ocean-atmosphere model were  
26 conducted by adding anomalous incoming solar radiation over the entire globe, Northern  
27 Hemisphere mid-latitudes, Southern Ocean, and tropics, respectively, with both positive and  
28 negative perturbation considered. The varied forcing patterns led to highly divergent climate  
29 sensitivities, with extratropical forcing inducing significantly more global-mean temperature  
30 change compared to tropical forcing. This dependence is particularly strong over the Southern  
31 Hemisphere, where the climate is nearly twice as sensitive to Southern Ocean forcing as tropical  
32 forcing. This dependence of climate sensitivity on the location of radiative forcing stems from  
33 covariations between lapse rate feedback, cloud feedback and tropospheric stability. These  
34 results contrast with the conventional SST-pattern effect in which tropical surface temperature  
35 changes regulate the climate sensitivity, and has important implications for geoengineering and  
36 understanding the mechanisms of paleoclimate change.

37

## 38 **1. Introduction**

39 A linear zero-dimensional energy balance model is a useful tool for understanding the  
40 relationship between radiative forcing and surface temperature. It provides a straightforward way  
41 to estimate climate sensitivity (Gregory et al., 2004). However, this framework does not account  
42 for the spatial pattern of surface temperature changes. The spatial pattern of sea surface  
43 temperature (SST) change has received much attention. Previous studies have shown that the  
44 spatial pattern of SST has great impacts on precipitation (Xie et al., 2010), large-scale circulation  
45 (Ma & Xie, 2013), global radiative budget and thus radiative feedbacks (Andrews et al., 2022;  
46 Andrews & Webb, 2018). In particular, the dependence of radiative feedbacks on SST spatial  
47 patterns is of great interest to the community (Andrews et al., 2015; Andrews & Webb, 2018), as  
48 model predicted climate sensitivity can vary considerably between different patterns of SST  
49 changes even though these patterns have the same global mean values (Zhao, 2022). To estimate  
50 the impacts of SST spatial patterns on climate feedback and sensitivity, recent studies have  
51 utilized a Green's function approach to analyze the climate response to local SST changes in  
52 atmosphere-only models forced by monthly-varying SST, and have shown that SST warming  
53 over tropical warm pools is associated with strong global-mean radiative cooling, whereas the  
54 same amount of SST warming over mid-to-high latitudes (e.g., the Southern Ocean) induces  
55 relatively small global-mean radiative response (Dong et al., 2019; Zhang et al., 2023; Zhou et  
56 al., 2017).

57 While the Green's function approach has shown to be useful in understanding the SST  
58 pattern effect on climate sensitivity, large uncertainties exist in terms of future SST projections.  
59 It is important to understand the radiative forcing pattern effect in atmosphere-ocean coupled  
60 models, where SST response to radiative forcing can be retrieved from such models. Motivated  
61 by the SST pattern effect on radiative feedbacks, this study seeks to explore how spatial  
62 asymmetries in radiative forcing influence climate sensitivity through a series of idealized solar  
63 forcing experiments using an atmosphere-ocean coupled system, which can help us understand  
64 the paleoclimate and guide the development of potential geoengineering strategies in the future.

65 Previous studies have examined impacts of forcing patterns on the climate system from  
66 different perspectives. For example, Stuecker et al. (2020) showed that both local and remote  
67 CO<sub>2</sub> forcing affect equatorial temperature via the large-scale atmospheric circulation like the

68 Hadley cell, the oceanic circulation, and local cloud feedback. Compared with tropical forcings,  
69 extratropical forcings have a greater impact on global temperature change (De F. Forster et al.,  
70 2000; Joshi et al., 2003). Similarly, ocean heat uptake in higher latitudes results in greater global  
71 surface temperature change than ocean heat uptake in lower latitudes, which is attributed to  
72 distinct cloud feedbacks and circulation changes (Kang & Xie, 2014; Liu et al., 2018; Rose et al.,  
73 2014; Rugenstein et al., 2016). Extratropical radiative forcings also shift the position of the  
74 intertropical convergence zone (ITCZ) by modifying the meridional energy transport (Kang et  
75 al., 2019; Xiang et al., 2018). From a paleoclimate perspective, variations in obliquity alter the  
76 meridional distribution of incoming solar radiation at TOA, which further affects SST and  
77 climate feedbacks (Mantsis et al., 2011), and large-scale circulation (Mantsis et al., 2014).  
78 Orbital precession can also change the energy budget at TOA, which impacts the Hadley cell  
79 (Merlis et al., 2013a, 2013b) and tropical precipitation (Merlis et al., 2013c).

80 In this study, we investigate the dependence of climate feedback and sensitivity on the  
81 spatial pattern of solar forcing in a coupled climate model. Specifically, the incoming solar  
82 radiation at TOA is perturbed at different geographic locations to mimic the effect of changes in  
83 the spatial pattern of radiative forcing. A series of perturbation experiments are conducted by  
84 imposing an abrupt change of incoming solar radiation over the entire globe, and three zonal  
85 bands including the Northern Hemisphere mid-latitudes, Southern Ocean, and tropics,  
86 respectively. These experiments reveal a strong dependence of climate sensitivity upon the  
87 spatial pattern of radiative forcing, with extratropical forcings inducing roughly twice as much  
88 global-mean temperature change as tropical forcings, particularly in the Southern Hemisphere.

## 89 **2. Methods**

### 90 **2.1 Idealized Spatial Patterns of Solar Forcing Perturbation**

91 Applying a fractional change to the solar constant is one approach of modifying incoming  
92 solar radiation. However, since the amplitude of annual mean incoming solar radiation peaks at  
93 the equator and decreases poleward, the resulting solar perturbation by this approach varies with  
94 latitude. This makes it challenging to determine whether the response is due to the amount of the  
95 fractional change, the spatial pattern of the perturbation, or a combination of both. The goal is to  
96 investigate the dependence of climate response on the location of anomalous incoming solar  
97 radiation. To achieve this, we impose solar forcing perturbation over the entire globe, Northern

98 Hemisphere Mid-latitudes, Southern Ocean, and Tropics. We seek to ensure that the annual mean  
 99 anomalies are horizontally uniform, thereby excluding any potential impacts from the  
 100 heterogeneity of imposed forcing within the regions of interest. By doing so, we can better  
 101 understand the dependence of climate response on the location of the forcing and its potential  
 102 implications for climate sensitivity.

103 Nadeau and McGehee (2017) showed that the annual mean distribution of incoming solar  
 104 radiation for the Earth can be estimated by a second-degree approximation:

$$\sigma_2(y, \beta) = 1 - \frac{5}{8} p_2(\cos \beta) p_2(y) \#(1)$$

105 where  $y$  stands for sine of latitude,  $\beta$  is obliquity,  $p_2(y)$  is the Legendre polynomials with  
 106  $p_2(y) = (3y^2 - 1)/2$ . A simplified version is provided by North (1975):

$$\hat{\sigma}_2(y) = 1 - 0.482 \times p_2(y) \#(2)$$

107 In this form, the annual mean distribution of incoming solar radiation is only a function of  
 108 latitude. We first normalize the instantaneous incoming solar radiation at each model time step  
 109 by the annual mean distribution of incoming solar radiation. The incoming solar radiation  
 110 perturbation is deduced by (i) applying a  $1 \text{ W m}^{-2}$  change to the solar constant over the perturbed  
 111 region to have a spatially and spectrally dependent forcing perturbation; (ii) dividing it by Eq. 2  
 112 to make it horizontally uniform (when integrated annually over the entire spectrum); and (iii)  
 113 multiplying it with a parameter to specify the global mean solar forcing perturbation. By doing  
 114 this, only the annual mean perturbation is horizontally uniform, whereas neither the  
 115 instantaneous nor the monthly mean perturbation is.

116 In this study, we consider both positive and negative perturbations. To ensure that the  
 117 experiments are comparable with each other for the same sign, we keep the absolute magnitude  
 118 of the global mean forcing the same. Since the domain size varies across the experiments, the  
 119 parameter used to control the magnitude depends on the domain size. Specifically, positive  
 120 perturbation experiments have a global mean forcing of  $+4 \text{ W m}^{-2}$  while the negative ones have  
 121 a global mean forcing of  $-4 \text{ W m}^{-2}$ . When the forcing is imposed over the entire globe, the  
 122 parameter is  $\pm 16.0$  given that the surface area of the globe is  $4\pi r^2$  but the effective area is  $\pi r^2$ ,  
 123 where  $r$  is the radius of the Earth. When adding forcing over a specific zonal band such as the  
 124 Northern Hemisphere Mid-latitudes ( $30^\circ\text{N}$  to  $60^\circ\text{N}$ ), we need to calculate the surface area of the

125 zonal band. To do this, we use the difference between the surface area of the bigger spherical cap  
126 (from the north pole to 30°N) and that of the smaller spherical cap (from the north pole to 60°N),  
127 which is given by:

$$2\pi r^2(1 - \sin \theta_1) - 2\pi r^2(1 - \sin \theta_2), \#(3)$$

128 where  $\theta_1 = 30^\circ$  and  $\theta_2 = 60^\circ$ . We use similar procedures to calculate the surface area for the  
129 Southern Ocean and Tropics. This approach ensures the same absolute values of global mean  
130 anomalous incoming solar radiation across all experiments and allows us to examine the climate  
131 response to forcing in a systematic way. The geographic locations of anomalous incoming solar  
132 radiation are shown in Figure S1. Note that neither global mean effective radiative forcing nor  
133 global mean instantaneous radiative forcing is supposed to be the same across all experiments by  
134 this approach.

## 135 **2.2 Model and Experiment**

136 The Seamless System for Prediction and Earth System Research (SPEAR), developed at  
137 NOAA's Geophysical Fluid Dynamics Laboratory (GFDL), is a fully atmosphere-ocean coupled  
138 model designed for physical climate prediction and projection over a range of timescales from  
139 seasonal to multidecadal (Delworth et al., 2020). In this study, the SPEAR\_LO version is used,  
140 which consists of AM4 for the atmosphere component and LM4 for the land component (Zhao et  
141 al., 2018a, 2018b). The atmosphere model has 33 vertical levels with a horizontal resolution of  
142 approximately 100 km. The ocean and sea ice components are based on the MOM6 model and  
143 have a nominal horizontal resolution of 1° and 75 vertical levels. Further information on the  
144 SPEAR\_LO can be found in Delworth et al. (2020).

145 In this study, a preindustrial control simulation integrated for 400 years is used as a base  
146 state, with radiative gas concentration and aerosol emission fixed at levels representative of the  
147 calendar year 1850. As noted in Delworth et al. (2020), this simulation displays a radiative  
148 imbalance at the TOA close to zero and little change in global mean surface air temperature over  
149 the 400-year period, indicating that the system is in near equilibrium. The climatological mean  
150 state is calculated from model outputs between years 101 and 300. For the perturbed simulations,  
151 initial conditions are retrieved from year 101 of the Control simulation, and an abrupt anomalous  
152 incoming solar radiation is added and maintained at a constant level throughout each simulation.

153 The domain of interest for each experiment is listed in Supplementary Table S1. Each perturbed  
154 simulation is integrated for 200 years.

### 155 **2.3 Radiative Kernel Analyses**

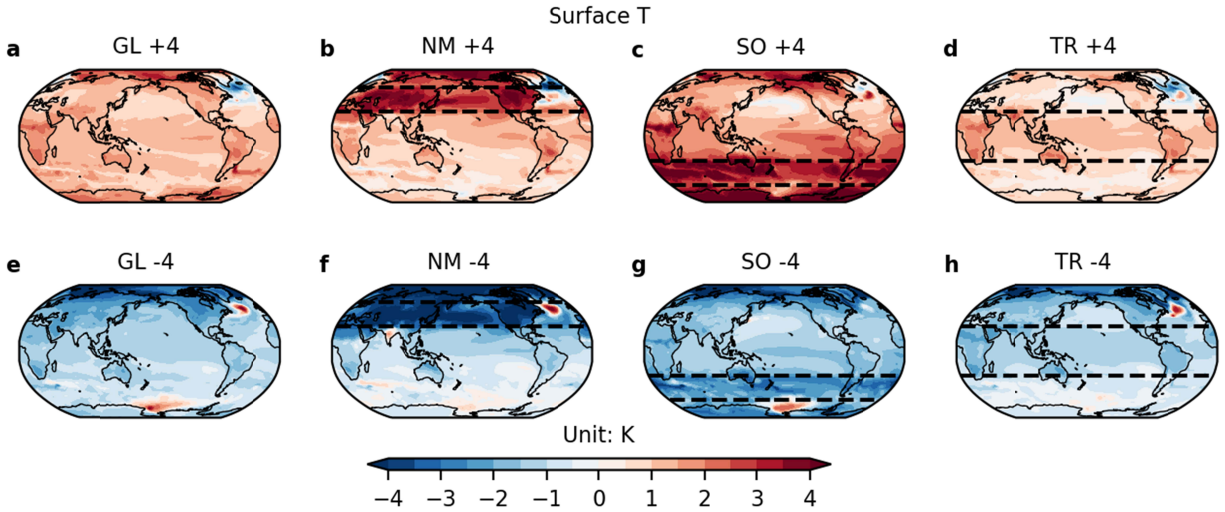
156 The radiative kernels used in this study are based on the atmospheric component of a  
157 recent generation climate model (HadGEM3) developed by the UK Met Office (Smith et al.,  
158 2020). The radiative kernel method decomposes the response of radiative fluxes at the TOA into  
159 individual components caused by changes in temperature, water vapor, surface albedo and  
160 clouds. Soden et al. (2008) showed that cloud feedback can be diagnosed from the response of  
161 cloud radiative effect corrected by cloud masking effect. The radiative kernel method quantifies  
162 radiative responses from changes in Planck (contributions of vertically uniform warming), lapse  
163 rate (contributions of departures from vertically uniform warming), water vapor, surface albedo,  
164 and cloudiness. Here we compute radiative feedbacks as the difference between Control  
165 climatology and the last 20 years of the perturbation experiments.

## 166 **3. Surface Temperature Response and Climate Sensitivity**

167 Figure 1 illustrates impacts of anomalous incoming solar radiation on surface temperature  
168 changes. The globally uniform positive forcing, GL +4, results in an overall surface warming  
169 except the north Atlantic high latitudes (Figure 1a). NM +4 leads to enhanced surface warming  
170 over the Northern Hemisphere continents and the north Pacific, whereas the north Atlantic high  
171 latitudes still exhibit anomalous surface cooling (Figure 1b). By contrast, SO +4 shows large  
172 surface warming not only over the entire Southern Ocean, but also over the tropical eastern  
173 Pacific and tropical Atlantic (Figure 1c). The teleconnection between the SO and the tropics  
174 involves several proposed mechanisms such as low cloud feedbacks (Kim et al., 2022; Zhang et  
175 al., 2021), and surface wind anomalies associated with the Antarctic ozone hole (Hartmann,  
176 2022). TR +4 exhibits a similar surface warming pattern as GL +4, but with a weaker magnitude  
177 (Figure 1d). The negative perturbation experiments show similar patterns of surface temperature  
178 changes as their positive counterparts, but with opposite signs (Figure 1e-h).

179





180

181 Figure 1 Maps of surface temperature changes (i.e., SST over ocean and surface skin temperature  
 182 over land; units: K) averaged over the last 50 years (year 151-200) of each simulation relative to  
 183 the base state of Control. The dashed lines in NM, SO, and TR mark the geographical boundaries  
 184 of the anomalous solar forcing imposed.

185 The distinctive SST responses over the north Atlantic high latitudes indicate changes in  
 186 the Atlantic Meridional Overturning Circulation (AMOC), which is tightly connected with the  
 187 SST changes over the north Atlantic (Zhang & Delworth, 2005). Previous modeling studies  
 188 reported a reduction in AMOC strength as the climate warms, which is due to an increase in local  
 189 surface heat fluxes and surface freshwater fluxes, although their relative importance varies  
 190 (Gregory et al., 2005; Weaver et al., 2007). A weakened AMOC is found to cause a cooling  
 191 tendency to the south of Greenland in the north Atlantic (Liu et al., 2020). Here we find that NM  
 192 +4 has the most reduction in the AMOC strength while NM -4 has the most increase (Figure S2),  
 193 which is consistent with the anomalous north Atlantic SST cooling in NM +4 and anomalous  
 194 warming in NM -4 as shown in Figure 1. While similar AMOC responses are found in GL and  
 195 TR cases, AMOC is hardly affected in SO cases (Figure S2), indicating that forcing over the  
 196 Southern Hemisphere mid-latitude may not alter transient AMOC strength very much, although  
 197 possible changes may appear with longer integration. Within the 200-year simulation, it is the  
 198 forcing in the Northern Hemisphere mid-latitude that greatly changes the AMOC strength.

199 Overall, the varied patterns of surface temperature responses in Figure 1 indicate  
 200 variations in climate sensitivity. Near the end of the simulations, the global mean temperature  
 201 change in SO cases is nearly twice as large as that in TR cases (Figure S3). Although the global  
 202 mean responses are not exactly symmetric between the positive and negative forcing

203 experiments, the dependence of climate sensitivity on the geographic locations of the imposed  
204 anomalous incoming solar radiation indicates robust *radiative forcing pattern effect*.

205 Previously Winton et al. (2010) introduced the ocean heat uptake efficacy factor ( $\epsilon$ ) to  
206 address climate response to an increase in CO<sub>2</sub> concentration. The efficacy factor was explained  
207 in the context of a two-box model by Held et al. (2010), and was used to account for the effect of  
208 evolving SST spatial patterns on climate feedback (Winton et al., 2020). Here, large values of  $\epsilon$   
209 are mainly found in TR (not shown), indicating strong damping of the imposed forcing and thus  
210 large negative radiative feedback, whereas small values of  $\epsilon$  mostly appear in extratropical  
211 forcing cases (NM and SO) and global forcing cases (GL), which suggests weak damping of the  
212 imposed forcing and thus small negative radiative feedback. In addition, as indicated by the time  
213 series of global mean surface air temperature (Figure S3), the negative perturbation experiments  
214 evolve toward equilibrium in a faster pace than the positive ones. Stouffer (2004) showed that  
215 the coupled system exhibits a shorter response time scale with an abrupt half of CO<sub>2</sub>  
216 concentration than an abrupt doubling of CO<sub>2</sub> concentration. Variations of the response times  
217 scale between positive and negative forcing suggest that one may not use the relationship found  
218 solely from either positive forcing or negative forcing experiments to constrain transient climate  
219 sensitivity (Merlis et al., 2014).

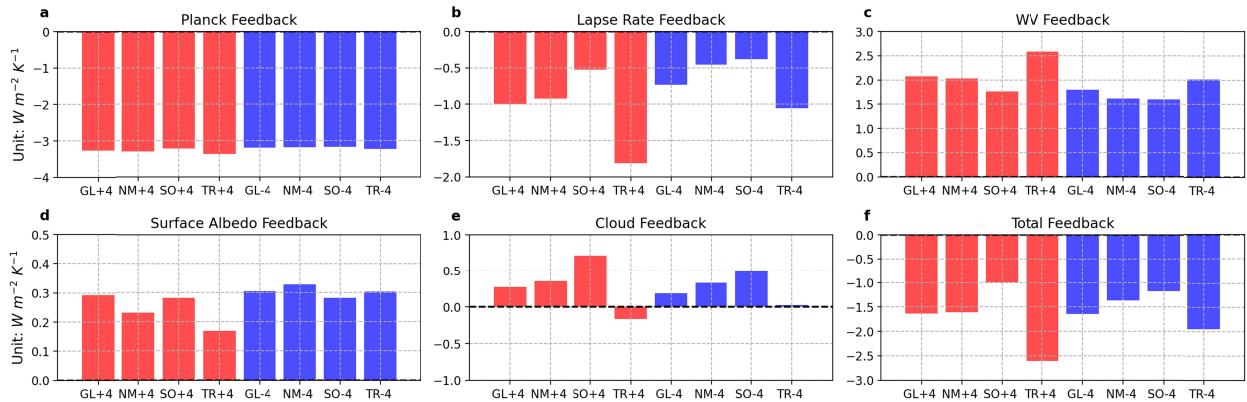
220

#### 221 **4. Radiative Feedbacks**

222 To understand solar forcing pattern effect, we diagnose radiative feedbacks using the  
223 radiative kernel method (see Methods). The Planck feedback is negative and shows relatively  
224 small variations across the perturbation experiments (Figure 2a). The lapse rate feedback is also  
225 negative but exhibits large variations (Figure 2b), which is primarily due to the distinctive  
226 surface warming patterns caused by changes in solar forcing location. The coupling between the  
227 surface and the free troposphere is strong in the tropics because of temperature response  
228 following a moist adiabat. Therefore, a relatively larger warming in the tropics is associated with  
229 more tropospheric warming, a greater reduction in lapse rate, and a more negative lapse rate  
230 feedback (Soden & Held, 2006). Here, the tropical forcing has relatively more warming at low  
231 latitudes and thus more negative lapse rate feedback. However, the extratropical forcing,  
232 especially for the SO forcing, has relatively more surface warming at high latitudes where the

233 surface-troposphere coupling is weak, which leads to a less negative lapse rate feedback (Figure  
 234 2b). Knowing the radiative forcing pattern effect on lapse rate feedback is important for  
 235 estimation of climate sensitivity given that it is hard to constrain lapse rate feedback based on  
 236 observations (He et al., 2021). Additionally, we note the positive forcing experiments tend to  
 237 have a larger lapse rate feedback than the negative forcing experiments. which is mainly due to  
 238 the increased moisture content as the climate warms. More water vapor means an increase in  
 239 latent heat release as parcels rise, which leads to a steeper moist adiabatic lapse rate (Held &  
 240 Soden, 2000). Indeed, the water vapor feedback is larger in the positive forcing experiment than  
 241 that in the negative forcing experiments (Figure 2c). An in-depth review of water vapor feedback  
 242 and lapse rate feedbacks can be found in Colman and Soden (2021). The surface albedo feedback  
 243 is positive too but is relatively small in magnitude (Figure 2d).

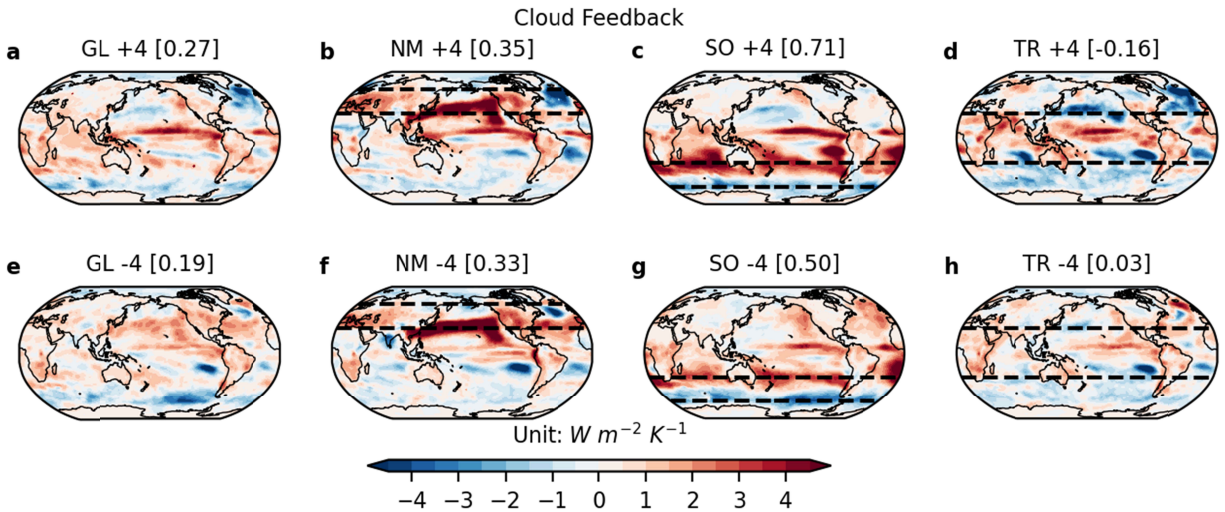
244 Not surprisingly, the range in cloud feedback is large between these experiments (Figure  
 245 2e). The cloud feedback in TR +4 is slightly negative and becomes almost zero in TR -4. By  
 246 contrast, large positive cloud feedback is found in SO cases. The large spread in cloud feedback  
 247 is reflected in the total radiative feedback, where TR +4 is roughly  $-2.5 \text{ W m}^{-2} \text{ K}^{-1}$  but SO +4 is  
 248 roughly  $-1.0 \text{ W m}^{-2} \text{ K}^{-1}$  (Figure 2f).



249  
 250  
 251 Figure 2 The global mean (a) Planck feedback, (b) lapse rate feedback, (c) water vapor feedback,  
 252 (d) surface albedo feedback, (e) cloud feedback, and (f) total radiative feedback (units:  $\text{W m}^{-2} \text{ K}^{-1}$ ).  
 253 Positive forcing experiments are in red while negative forcing experiments are in blue.

254 Maps of local cloud feedback (i.e., cloud induced radiative perturbations at TOA  
 255 corrected by cloud masking effect and then divided by global mean surface air temperature  
 256 change) are shown in Figure 3. For TR cases, negative values in the extratropics and positive  
 257 values in the deep tropics tend to offset, leading to a slightly negative global mean cloud

258 feedback in TR +4 (Figure 3d) and nearly zero one in TR -4 (Figure 3h). For SO cases, positive  
 259 values are found mostly over tropical and subtropical oceans, especially over the stratocumulus-  
 260 dominated areas such as the southeastern Pacific and Atlantic (Figure 3c and Figure 3g). In terms  
 261 of NM cases, positive values mainly appear over the north Pacific (Figure 3b and Figure 3f).  
 262 Such patterns yield an overall more positive global mean cloud feedback.

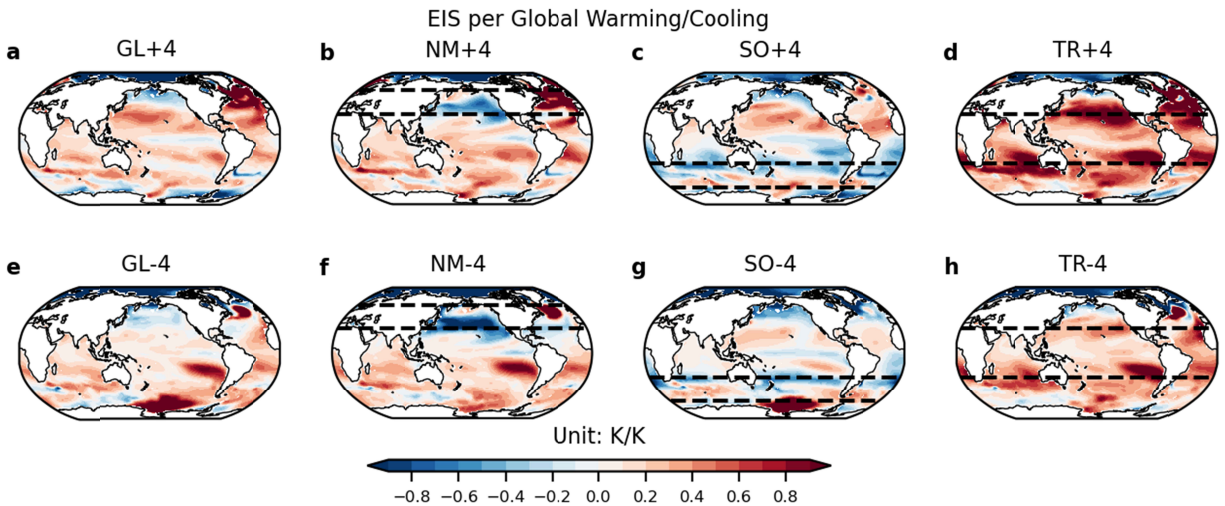


263  
 264 Figure 3 Maps of local cloud feedback (units:  $W m^{-2} K^{-1}$ ). The global mean values are listed in  
 265 the square brackets.  
 266

## 267 5. Connection to Cloud Controlling Factors

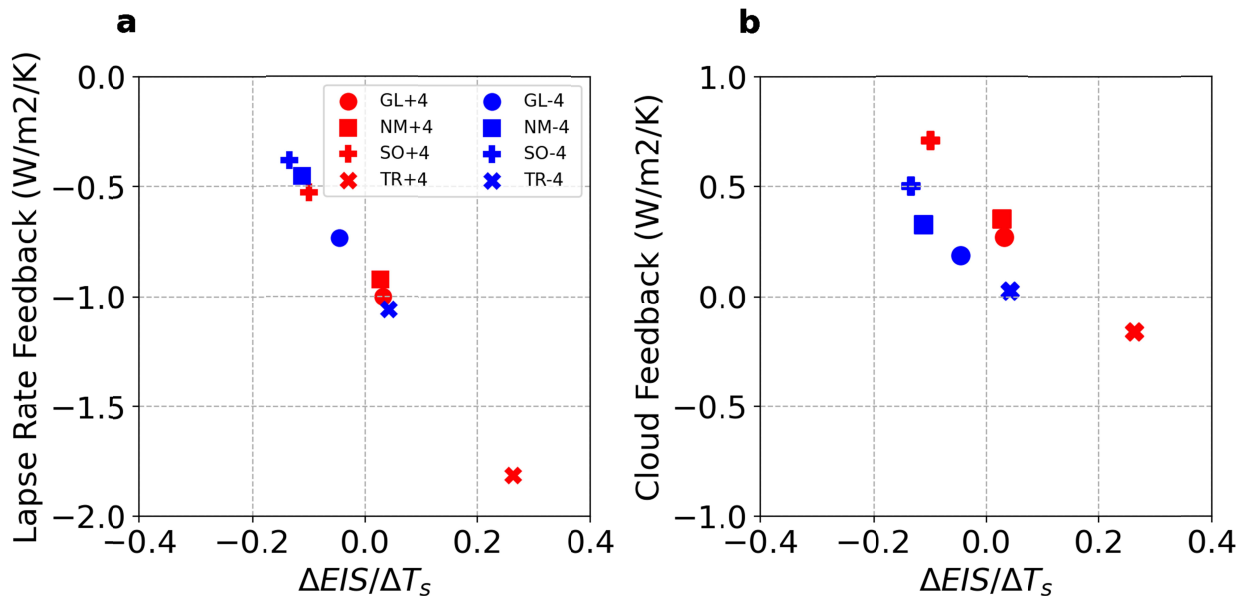
268 Then the question is: why changes in the forcing location alter the sign and magnitude of  
 269 cloud feedback? Recent studies proposed that meteorological cloud-controlling factors like SST,  
 270 estimated inversion strength (Wood & Bretherton, 2006) among other variables can explain  
 271 changes in cloud amount and thus cloud feedback, especially low cloud feedback (Myers et al.,  
 272 2021; Scott et al., 2020). Among the proposed cloud-controlling factors, we find that estimated  
 273 inversion strength (EIS) is a primary factor affecting cloud feedback. Here, changes in EIS are  
 274 normalized by global mean temperature changes (Figure 4) to allow for a direct comparison with  
 275 cloud feedback. Large positive values are found in TR cases, indicating a more stable  
 276 troposphere in a warmer climate that favors more low cloud amount, and results in enhanced  
 277 radiative cooling and negative cloud feedback in the subtropics (Figure 3d and Figure 3h). In  
 278 comparison, the EIS response in NM and SO cases show interhemispheric asymmetry. Negative  
 279 values are mostly found in the forcing domain, which indicates locally decreased stability in a

280 warmer climate. As a result, positive cloud feedback becomes dominant and contributes to the  
 281 overall positive global mean cloud feedback in NM and SO cases (Figure 3b and Figure 3f).  
 282



283  
 284 Figure 4 Maps of changes in EIS per degree of global mean temperature change (units:  $K K^{-1}$ ).

285 The changes in EIS covary with the changes in lapse rate feedback. A more negative  
 286 lapse rate feedback means relatively more tropospheric warming than surface warming, which  
 287 tends to enhance the tropospheric stability (Figure 5a). The increased tropospheric stability  
 288 favors more cloud and thus leads to a more negative cloud feedback (Figure 5b). Also, the  
 289 positive forcing experiments tend to have larger lapse rate and EIS response than the negative  
 290 forcing experiments because of the moist adiabat dependence on temperature.



291

292 Figure 5 Scatterplots of (a) changes in global mean EIS per degree of global mean temperature  
293 change (units:  $\text{K K}^{-1}$ ) versus lapse rate feedback, and (b) changes in EIS per degree of global  
294 mean temperature change (units:  $\text{K K}^{-1}$ ) versus cloud feedback.

## 295 **6. Discussions and Summary**

296 This study investigates how changes in locations of imposed solar forcing affect the  
297 climate system in an atmosphere-ocean coupled model. We conduct a series of sensitivity  
298 experiments where anomalous incoming solar radiation is imposed globally and over three zonal  
299 bands including the Northern Hemisphere mid-latitudes, Southern Ocean, and tropics,  
300 respectively. Our analyses show that extratropical forcing results in larger temperature change  
301 compared to tropical forcing. The range in climate sensitivity mainly stems from variations in  
302 lapse rate feedback and cloud feedback, in which both are related to changes in tropospheric  
303 stability.

304 Our results have implications for historical aerosol forcing, volcanic eruptions, and  
305 potential geoengineering efforts in the future. Compared to the idealized solar forcing  
306 experiments, aerosol forcing involves larger spatial-temporal variability. Over the historical  
307 period, changes in anthropogenic aerosols play an important role in altering radiative forcing,  
308 which is mostly due to a geographic shift of major aerosol emission sources. The spatial  
309 distribution of aerosols impacts surface temperature responses as shown in Persad and Caldeira  
310 (2018). In addition, volcanic eruptions can also induce an abrupt change in the geographic  
311 distribution of aerosols, which can further affect the mean state of the climate system (Yang et  
312 al., 2019). As indicated by the simulations, zonally symmetric forcing in the extratropics induces  
313 larger global mean temperature changes than that in the tropics. This implies that the  
314 effectiveness of geoengineering in modifying the overall mean state of the climate system would  
315 be limited if the forcing is applied solely over the tropics. Alternatively, our results highlight the  
316 importance of carefully choosing the location of the forcing when developing and evaluating  
317 potential geoengineering strategies.

318 Overall, the results in this study provide evidence of the solar forcing pattern effect on the  
319 climate system, which involves dependence of radiative feedbacks on the geographic locations of  
320 solar forcing. Considering the computational cost of running coupled climate models, we only  
321 apply zonally symmetric forcing over the entire globe and three individual zonal bands, and  
322 perturb the entire shortwave spectrum of the solar radiation. We acknowledge that the solar

323 forcing's spatial pattern can be more complex. Also, the perturbation is applied to the entire  
324 spectrum of solar radiation. A recent study suggested that the impact of solar radiation is  
325 spectrally dependent (Jing et al., 2021). While these issues are beyond the scope of this study, we  
326 suggest that future research could explore related questions, building on our findings to gain a  
327 more comprehensive understanding of the multifaceted interactions between external radiative  
328 forcing, feedback, surface temperature, and other aspects of the climate system.

## 329 **Acknowledgments**

330 We thank Timothy Merlis, Leo Donner, and Isaac Held for suggestions and comments on  
331 the initial draft of this paper. Support from NOAA OAR and GFDL leadership for this project is  
332 acknowledged.

## 333 **Open Research**

334 The data archiving is underway. Parts of the data have been uploaded to Zenodo  
335 (<https://zenodo.org/record/8156740>).

## 336 **References**

- 337 Andrews, T., Bodas-Salcedo, A., Gregory, J. M., Dong, Y., Armour, K. C., Paynter, D., et al. (2022). On the effect  
338 of historical SST patterns on radiative feedback. *Journal of Geophysical Research: Atmospheres*, 127(18),  
339 e2022JD036675.
- 340 Andrews, T., Gregory, J. M., & Webb, M. J. (2015). The dependence of radiative forcing and feedback on evolving  
341 patterns of surface temperature change in climate models. *Journal of Climate*, 28(4), 1630-1648.
- 342 Andrews, T., & Webb, M. J. (2018). The dependence of global cloud and lapse rate feedbacks on the spatial  
343 structure of tropical Pacific warming. *Journal of Climate*, 31(2), 641-654.
- 344 Colman, R., & Soden, B. J. (2021). Water vapor and lapse rate feedbacks in the climate system. *Reviews of Modern  
345 Physics*, 93(4), 045002.
- 346 de F. Forster, P., Blackburn, M., Glover, R., & Shine, K. (2000). An examination of climate sensitivity for idealised  
347 climate change experiments in an intermediate general circulation model. *Climate Dynamics*, 16, 833-849.
- 348 Delworth, T. L., Cooke, W. F., Adcroft, A., Bushuk, M., Chen, J. H., Dunne, K. A., et al. (2020). SPEAR: The next  
349 generation GFDL modeling system for seasonal to multidecadal prediction and projection. *Journal of  
350 Advances in Modeling Earth Systems*, 12(3), e2019MS001895.
- 351 Dong, Y., Proistosescu, C., Armour, K. C., & Battisti, D. S. (2019). Attributing historical and future evolution of  
352 radiative feedbacks to regional warming patterns using a Green's function approach: The preeminence of  
353 the western Pacific. *Journal of Climate*, 32(17), 5471-5491.
- 354 Gregory, J., Dixon, K., Stouffer, R., Weaver, A., Driesschaert, E., Eby, M., et al. (2005). A model intercomparison  
355 of changes in the Atlantic thermohaline circulation in response to increasing atmospheric CO2  
356 concentration. *Geophysical Research Letters*, 32(12).
- 357 Gregory, J., Ingram, W., Palmer, M., Jones, G., Stott, P., Thorpe, R., et al. (2004). A new method for diagnosing  
358 radiative forcing and climate sensitivity. *Geophysical Research Letters*, 31(3).
- 359 Hartmann, D. L. (2022). The Antarctic ozone hole and the pattern effect on climate sensitivity. *Proceedings of the  
360 National Academy of Sciences*, 119(35), e2207889119.
- 361 He, H., Kramer, R. J., & Soden, B. J. (2021). Evaluating Observational Constraints on Intermodel Spread in Cloud,  
362 Temperature, and Humidity Feedbacks. *Geophysical Research Letters*, 48(17), e2020GL092309.
- 363 Held, I. M., & Soden, B. J. (2000). Water vapor feedback and global warming. *Annual review of energy and the  
364 environment*, 25(1), 441-475.
- 365 Held, I. M., Winton, M., Takahashi, K., Delworth, T., Zeng, F., & Vallis, G. K. (2010). Probing the fast and slow  
366 components of global warming by returning abruptly to preindustrial forcing. *Journal of Climate*, 23(9),  
367 2418-2427.

368 Jing, X., Huang, X., Chen, X., Wu, D. L., Pilewskie, P., Coddington, O., & Richard, E. (2021). Direct influence of  
369 solar spectral irradiance on the high-latitude surface climate. *Journal of Climate*, 34(10), 4145-4158.

370 Joshi, M., Shine, K., Ponater, M., Stuber, N., Sausen, R., & Li, L. (2003). A comparison of climate response to  
371 different radiative forcings in three general circulation models: towards an improved metric of climate  
372 change. *Climate Dynamics*, 20, 843-854.

373 Kang, S. M., Hawcroft, M., Xiang, B., Hwang, Y.-T., Cazes, G., Codron, F., et al. (2019). Extratropical–tropical  
374 interaction model intercomparison project (ETIN-MIP): Protocol and initial results. *Bulletin of the  
375 American Meteorological Society*, 100(12), 2589-2606.

376 Kang, S. M., & Xie, S.-P. (2014). Dependence of climate response on meridional structure of external thermal  
377 forcing. *Journal of Climate*, 27(14), 5593-5600.

378 Kim, H., Kang, S. M., Kay, J. E., & Xie, S.-P. (2022). Subtropical clouds key to Southern Ocean teleconnections to  
379 the tropical Pacific. *Proceedings of the National Academy of Sciences*, 119(34), e2200514119.

380 Liu, F., Lu, J., Garuba, O. A., Huang, Y., Leung, L. R., Harrop, B. E., & Luo, Y. (2018). Sensitivity of surface  
381 temperature to oceanic forcing via q-flux green's function experiments. Part II: feedback decomposition  
382 and polar amplification. *Journal of Climate*, 31(17), 6745-6761.

383 Liu, W., Fedorov, A. V., Xie, S.-P., & Hu, S. (2020). Climate impacts of a weakened Atlantic Meridional  
384 Overturning Circulation in a warming climate. *Science advances*, 6(26), eaaz4876.

385 Ma, J., & Xie, S.-P. (2013). Regional patterns of sea surface temperature change: A source of uncertainty in future  
386 projections of precipitation and atmospheric circulation. *Journal of Climate*, 26(8), 2482-2501.

387 Mantsis, D. F., Clement, A. C., Broccoli, A. J., & Erb, M. P. (2011). Climate feedbacks in response to changes in  
388 obliquity. *Journal of Climate*, 24(11), 2830-2845.

389 Mantsis, D. F., Lintner, B. R., Broccoli, A. J., Erb, M. P., Clement, A. C., & Park, H.-S. (2014). The response of  
390 large-scale circulation to obliquity-induced changes in meridional heating gradients. *Journal of Climate*,  
391 27(14), 5504-5516.

392 Merlis, T. M., Held, I. M., Stenchikov, G. L., Zeng, F., & Horowitz, L. W. (2014). Constraining transient climate  
393 sensitivity using coupled climate model simulations of volcanic eruptions. *Journal of Climate*, 27(20),  
394 7781-7795.

395 Merlis, T. M., Schneider, T., Bordoni, S., & Eisenman, I. (2013a). Hadley circulation response to orbital precession.  
396 Part I: Aquaplanets. *Journal of Climate*, 26(3), 740-753.

397 Merlis, T. M., Schneider, T., Bordoni, S., & Eisenman, I. (2013b). Hadley circulation response to orbital precession.  
398 Part II: Subtropical continent. *Journal of Climate*, 26(3), 754-771.

399 Merlis, T. M., Schneider, T., Bordoni, S., & Eisenman, I. (2013c). The tropical precipitation response to orbital  
400 precession. *Journal of Climate*, 26(6), 2010-2021.

401 Myers, T. A., Scott, R. C., Zelinka, M. D., Klein, S. A., Norris, J. R., & Caldwell, P. M. (2021). Observational  
402 constraints on low cloud feedback reduce uncertainty of climate sensitivity. *Nature Climate Change*, 11(6),  
403 501-507.

404 Nadeau, A., & McGehee, R. (2017). A simple formula for a planet's mean annual insolation by latitude. *Icarus*, 291,  
405 46-50.

406 North, G. R. (1975). Analytical solution to a simple climate model with diffusive heat transport. *Journal of  
407 Atmospheric Sciences*, 32(7), 1301-1307.

408 Persad, G. G., & Caldeira, K. (2018). Divergent global-scale temperature effects from identical aerosols emitted in  
409 different regions. *Nature communications*, 9(1), 3289.

410 Rose, B. E., Armour, K. C., Battisti, D. S., Feldl, N., & Koll, D. D. (2014). The dependence of transient climate  
411 sensitivity and radiative feedbacks on the spatial pattern of ocean heat uptake. *Geophysical Research  
412 Letters*, 41(3), 1071-1078.

413 Rugenstein, M. A., Caldeira, K., & Knutti, R. (2016). Dependence of global radiative feedbacks on evolving  
414 patterns of surface heat fluxes. *Geophysical Research Letters*, 43(18), 9877-9885.

415 Scott, R. C., Myers, T. A., Norris, J. R., Zelinka, M. D., Klein, S. A., Sun, M., & Doelling, D. R. (2020). Observed  
416 sensitivity of low-cloud radiative effects to meteorological perturbations over the global oceans. *Journal of  
417 Climate*, 33(18), 7717-7734.

418 Smith, C. J., Kramer, R. J., & Sima, A. (2020). The HadGEM3-GA7. 1 radiative kernel: the importance of a well-  
419 resolved stratosphere. *Earth System Science Data*, 12(3), 2157-2168.

420 Soden, B. J., & Held, I. M. (2006). An assessment of climate feedbacks in coupled ocean–atmosphere models.  
421 *Journal of Climate*, 19(14), 3354-3360.

422 Soden, B. J., Held, I. M., Colman, R., Shell, K. M., Kiehl, J. T., & Shields, C. A. (2008). Quantifying climate  
423 feedbacks using radiative kernels. *Journal of Climate*, 21(14), 3504-3520.



424 Stouffer, R. J. (2004). Time scales of climate response. *Journal of Climate*, 17(1), 209-217.

425 Stuecker, M. F., Timmermann, A., Jin, F.-F., Proistosescu, C., Kang, S. M., Kim, D., et al. (2020). Strong remote  
426 control of future equatorial warming by off-equatorial forcing. *Nature Climate Change*, 10(2), 124-129.

427 Weaver, A. J., Eby, M., Kienast, M., & Saenko, O. A. (2007). Response of the Atlantic meridional overturning  
428 circulation to increasing atmospheric CO<sub>2</sub>: Sensitivity to mean climate state. *Geophysical Research  
429 Letters*, 34(5).

430 Winton, M., Adcroft, A., Dunne, J., Held, I., Shevliakova, E., Zhao, M., et al. (2020). Climate sensitivity of GFDL's  
431 CM4. 0. *Journal of Advances in Modeling Earth Systems*, 12(1), e2019MS001838.

432 Winton, M., Takahashi, K., & Held, I. M. (2010). Importance of ocean heat uptake efficacy to transient climate  
433 change. *Journal of Climate*, 23(9), 2333-2344.

434 Wood, R., & Bretherton, C. S. (2006). On the relationship between stratiform low cloud cover and lower-  
435 tropospheric stability. *Journal of Climate*, 19(24), 6425-6432.

436 Xiang, B., Zhao, M., Ming, Y., Yu, W., & Kang, S. M. (2018). Contrasting impacts of radiative forcing in the  
437 Southern Ocean versus southern tropics on ITCZ position and energy transport in one GFDL climate  
438 model. *Journal of Climate*, 31(14), 5609-5628.

439 Xie, S.-P., Deser, C., Vecchi, G. A., Ma, J., Teng, H., & Wittenberg, A. T. (2010). Global warming pattern  
440 formation: Sea surface temperature and rainfall. *Journal of Climate*, 23(4), 966-986.

441 Yang, W., Vecchi, G. A., Fueglistaler, S., Horowitz, L. W., Luet, D. J., Muñoz, Á. G., et al. (2019). Climate impacts  
442 from large volcanic eruptions in a high-resolution climate model: The importance of forcing structure.  
443 *Geophysical Research Letters*, 46(13), 7690-7699.

444 Zhang, B., Zhao, M., & Tan, Z. (2023). Using a Green's function approach to diagnose the pattern effect in GFDL  
445 AM4 and CM4. *Journal of Climate*, 36(4), 1105-1124.

446 Zhang, R., & Delworth, T. L. (2005). Simulated tropical response to a substantial weakening of the Atlantic  
447 thermohaline circulation. *Journal of Climate*, 18(12), 1853-1860.

448 Zhang, X., Deser, C., & Sun, L. (2021). Is there a tropical response to recent observed Southern Ocean cooling?  
449 *Geophysical Research Letters*, 48(5), e2020GL091235.

450 Zhao, M. (2022). An investigation of the effective climate sensitivity in GFDL's new climate models CM4. 0 and  
451 SPEAR. *Journal of Climate*, 1-62.

452 Zhao, M., Golaz, J. C., Held, I., Guo, H., Balaji, V., Benson, R., et al. (2018a). The GFDL global atmosphere and  
453 land model AM4. 0/LM4. 0: 1. Simulation characteristics with prescribed SSTs. *Journal of Advances in  
454 Modeling Earth Systems*, 10(3), 691-734.

455 Zhao, M., Golaz, J. C., Held, I., Guo, H., Balaji, V., Benson, R., et al. (2018b). The GFDL global atmosphere and  
456 land model AM4. 0/LM4. 0: 2. Model description, sensitivity studies, and tuning strategies. *Journal of  
457 Advances in Modeling Earth Systems*, 10(3), 735-769.

458 Zhou, C., Zelinka, M. D., & Klein, S. A. (2017). Analyzing the dependence of global cloud feedback on the spatial  
459 pattern of sea surface temperature change with a Green's function approach. *Journal of Advances in  
460 Modeling Earth Systems*, 9(5), 2174-2189.

461